



HAL
open science

Diffuse field cross-correlation in a programmable-metasurface-stirred reverberation chamber

Philipp del Hougne, Jérôme Sol, Fabrice Mortessagne, Ulrich Kuhl, Olivier Legrand, Philippe Besnier, Matthieu Davy

► **To cite this version:**

Philipp del Hougne, Jérôme Sol, Fabrice Mortessagne, Ulrich Kuhl, Olivier Legrand, et al.. Diffuse field cross-correlation in a programmable-metasurface-stirred reverberation chamber. *Applied Physics Letters*, 2021, 118 (10), pp.104101. 10.1063/5.0039596 . hal-03189023

HAL Id: hal-03189023

<https://hal.science/hal-03189023>

Submitted on 22 Jun 2021

HAL is a multi-disciplinary open access archive for the deposit and dissemination of scientific research documents, whether they are published or not. The documents may come from teaching and research institutions in France or abroad, or from public or private research centers.

L'archive ouverte pluridisciplinaire **HAL**, est destinée au dépôt et à la diffusion de documents scientifiques de niveau recherche, publiés ou non, émanant des établissements d'enseignement et de recherche français ou étrangers, des laboratoires publics ou privés.

Diffuse Field Cross-Correlation in a Programmable-Metasurface-Stirred Reverberation Chamber

Philipp del Hougne,^{1,2} Jérôme Sol,¹ Fabrice Mortessagne,² Ulrich Kuhl,² Olivier Legrand,² Philippe Besnier,¹ and Matthieu Davy¹

¹Univ Rennes, INSA Rennes, CNRS, IETR - UMR 6164, F-35000, Rennes, France

²Université Côte d'Azur, CNRS, Institut de Physique de Nice - UMR 7010, 06108 Nice, France

Programmable metasurfaces can endow complex scattering environments with reconfigurability. Here, we make use of these configurational degrees of freedom to retrieve the impulse response between two passive antennas via cross-correlation techniques. An ensemble of stirred chaotic wave fields in a reverberation chamber (RC) can play the role of thermal noise in passive Green's function retrieval. Instead of using a conventional mechanical mode stirrer, we generate the ensemble of RC configurations with random configurations of a programmable metasurface. We adapt the data processing of the diffuse field cross-correlation technique to this stirring mechanism which is, given the size of the RC, nominally inefficient and we investigate the convergence of the cross-correlated signals toward the impulse response. Finally, we apply our scheme to phaseless imaging in complex propagation environments, with potential applications in indoor context-awareness.

Programmable metasurfaces¹⁻⁶, thin arrays of meta-atoms with multiple digitalized states corresponding to distinct electromagnetic responses, are a relatively young member of the family of artificial materials⁷⁻⁹. Nonetheless, they are at the forefront of real-life applications based on metamaterials, owing both to the ease of fabricating such thin structures and to their unique capability to manipulate electromagnetic fields in a reprogrammable manner. Although so far the majority of the literature considers applications of programmable metasurfaces in free space^{10,11}, their ability to endow complex scattering environments with "programmability" becomes increasingly important. On the one hand, optimized configurations can be used to engineer the propagation medium, enabling the study of fundamental wave-physics phenomena¹²⁻¹⁴ as well as new concepts in wireless communication¹⁵⁻¹⁷, energy harvesting¹⁸ and analog computing¹⁹. On the other hand, random configurations can be used for electronic stirring²⁰⁻²² in order to access configurational degrees of freedom, which has proven useful in sensing applications²³⁻²⁵.

To date, the opportunity to leverage the ability of programmable complex environments to generate an ensemble of spatially isotropic fields (in a statistical sense) for passive Green's function retrieval remains unexplored. Diffuse-field cross-correlation (DFCC) techniques were originally pioneered in acoustics^{26,27} and seismology²⁸ where received signals due to thermal fluctuations or earthquakes were correlated to retrieve the impulse response between passive antennas – without actively emitting a signal. The DFCC concept was also transposed to the electromagnetic domain²⁹ where one can conveniently replace the multitude of ambient noise sources with an ensemble of diffuse fields generated by a single source for different configurations of a chaotic reverberation chamber (RC)³⁰. Multiple scattering within a chaotic cavity indeed generates an isotropic random wavefield with Gaussian statistics³¹⁻³³ which enhances the convergence of the cross-correlation function towards the imaginary part of the Green's function between the two receivers^{26,34-41}. An RC hence constitutes an attractive solution for the fast characterization of integrated antenna arrays that can only be deployed

in receive mode.

In this Letter, we hence study DFCC in a chaotic RC stirred with programmable metasurfaces. In contrast to mechanical stirring²¹, using random configurations of programmable metasurfaces that only cover a small fraction of the RC surface constitutes a nominally inefficient stirring mechanism; therefore, we discuss how DFCC data processing can be adapted to inefficient stirring before thoroughly characterizing this route toward passive Green's function retrieval and reporting an application thereof to phaseless imaging.

Our experimental setup, depicted in Fig. 1(a), consists of an irregularly shaped metallic enclosure termed RC with a volume of 5.25 m³ and a quality factor of roughly 6600. The two horn antennas under test (indexed 1 and 2) are placed inside the RC, facing each other, such that there is a strong line-of-sight component in their transmission. A discone antenna (indexed 3) acts as source to excite the RC between 4.5 and 9 GHz. Two metasurfaces provide a total of 152 programmable meta-atoms. Each meta-atom has, independently for two field polarizations, two digitalized states ("0" and "1"), corresponding to two opposite electromagnetic responses. Given our use of the programmable metasurface for field stirring, the detailed characteristics of the responses are irrelevant; nonetheless, the general idea behind the design of the meta-atoms is to implement two states with a phase difference of roughly π at the central operating frequency around 5.1 GHz. Since the underlying working principle (detailed in Ref.⁴ and the SM) builds upon a resonant phenomenon, the operating bandwidth is inherently limited.

We now briefly discuss some essential aspects about conventional DFCC data processing. The fundamental operation in DFCC is the cross-correlation of the field $\psi(r, f)$ probed at two positions: $C(r_1, r_2, f) = \psi(r_1, f)\psi^*(r_2, f)$. The fluctuation-dissipation theorem shows that the average cross-correlation of an equipartitioned field probed with noninvasive pointlike receivers converges towards the real part of the mutual impedance $Z_{12}(f)$ between the ports⁴² or, equivalently, to the imaginary part of the Green's function between the two probes: $C(r_1, r_2, f) \propto \text{Im}[G(r_1, r_2, f)]$. Thus, the impulse re-

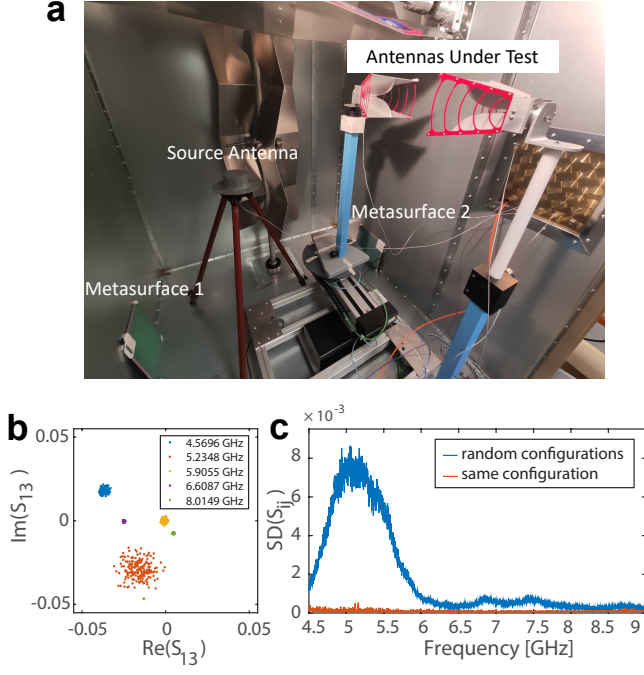


FIG. 1. (a) Experimental setup: A discone antenna (CMA-118-A) excites an irregularly shaped RC ($1.75 \times 1.50 \times 2.00 \text{ m}^3$, $Q \sim 6600$). Two horn antennas under test (ETS-3115) receive the reverberating waves. Two programmable metasurfaces locally tune the RC's boundary conditions. The mechanical mode stirrers seen in the photo are static throughout the experiment. (b) Clouds of $S_{13}(f_0)$ for 300 random configurations of the programmable metasurface at different frequencies f_0 . (c) Standard deviation of $S_{13}(f_0)$ as a function of f_0 for 300 measurements with random metasurface configurations. The same quantity is also plotted for 300 measurements with the same metasurface configuration to characterize the experimental noise.

response between two broadband receivers can be reconstructed passively. Such an equipartitioned field can also be obtained using noise sources uniformly distributed within the medium. Here, the sources are transmitting antennas located within a chaotic RC and we cross-correlate the complex transmission coefficients $S_{1m}(f)$ and $S_{2m}(f)$ between the two receiving antennas and M sources: $C_{\text{corr}}(f) = \sum_{m=3}^{M+2} S_{1m}(f)S_{2m}^*(f)$. Because the field within chaotic cavities is naturally random, depolarized and statistically uniform, the cross-correlation function is expected to provide the impulse response between the receivers even with a single or a few sources. The recovered signal $C_{\text{corr}}(f)$ for matched electromagnetic antennas is however not directly equivalent to the transmission $S_{12}(f)$ between the two antennas under test but influenced by each antenna's reflection coefficient³⁰. To illustrate this effect, let us first assume for simplicity that there is no absorption such that the overall system's scattering matrix S of the $M+2$ antennas is unitary: $SS^\dagger = \mathbb{1}$. This condition then leads to

$$\sum_{m=3}^{M+2} S_{1m}S_{2m}^* = -[S_{21}^*S_{11} + S_{12}S_{22}^*]. \quad (1)$$

In our case, we compute the correlation with a single source ($M = 1$) in a cavity with absorption. Absorption can be interpreted as the presence of additional fictitious channels that are

not included in the measured scattering matrix. The unitarity of S is therefore not satisfied. Nevertheless, this loss of information may be compensated to a large extent by averaging the correlation over an ensemble of random RC configurations, denoted by $\langle \dots \rangle$:

$$C_{\text{corr}}(f) = \langle S_{13}(f)S_{23}^*(f) \rangle. \quad (2)$$

Even though some details of the cross-correlation corresponding to the unitary case may be lost, we expect that the ballistic components of $C_{\text{corr}}(f)$ converge toward the ones of

$$C_0(f) = -\langle S_{21}^*(f)S_{11}(f) + S_{12}(f)S_{22}^*(f) \rangle \quad (3)$$

because the correlation in disordered and chaotic environments tends to be self-averaging at short times^{34,38}. In the following, we will use $C_0(f)$ as benchmark to which we can compare our retrieved signal $C_{\text{corr}}(f)$.

In contrast to conventional mechanical mode stirring, we are confronted with two challenges due to the limited size of our programmable metasurfaces: (i) the persistence of a strong unstirred field component, and (ii) the strong frequency dependence of the amplitude distribution of the stirred field component. The independence of the random fields to average the correlation may therefore not be satisfied so that $C_0(f)$ cannot be obtained from the correlation of the raw transmission data. To characterize the efficiency of programmable-metasurface-based electronic stirring, we acquire with a vector network analyzer (VNA) the transmission between the source antenna and one of the antennas under test for 300 random metasurface configurations between 4.5 and 9 GHz. In Fig. 1(b) we plot the corresponding clouds of $S_{13}(f_0)$ at a few selected frequencies in the complex plane. The frequency-dependent size of the clouds already hints at a strong frequency dependence of the stirring efficiency. Moreover, we observe that the clouds are in general not centered on the origin, giving rise to a substantial unstirred field component⁴³. To evaluate the stirring efficiency's frequency dependence more systematically, we plot in Fig. 1(c) the standard deviation of $S_{13}(f_0)$ as a function of f_0 . The central operating frequency around 5.1 GHz as well as a bandwidth of roughly 400 MHz clearly emerge from that plot. As reference, we also plot the noise baseline (evaluated for 300 measurements with the same metasurface configuration). We estimate that the ratio of unstirred to stirred components $|\langle S_{13}(f) \rangle|^2 / \langle |S_{13}(f)|^2 \rangle$ is 0.92 at $f = 5$ GHz and 0.999 at 6.5 GHz.

We now detail how we can adapt the DFCC technique to overcome these hurdles originating from our unconventional stirring mechanism. First, we remove the unstirred field components from $S_{13}(f)$ and $S_{23}(f)$ by using $S'_{13}(f) = S_{13}(f) - \langle S_{13}(f) \rangle$ and $S'_{23}(f) = S_{23}(f) - \langle S_{23}(f) \rangle$ instead. This step crucially relies on the excellent dynamic range of standard measurement equipment such as VNAs since the unstirred field component is significantly stronger than the stirred component in our experiment – see Fig. 1(b). Moreover, while $S'_{13}(f)$ and $S'_{23}(f)$ emulate a spatially isotropic source distribution, the amplitudes of $S'_{13}(f) - \langle S'_{13}(f) \rangle$ and $S'_{23}(f) - \langle S'_{23}(f) \rangle$ are peaked on the frequency range over which the metasurfaces are most efficient, as seen in Fig. 1(c).

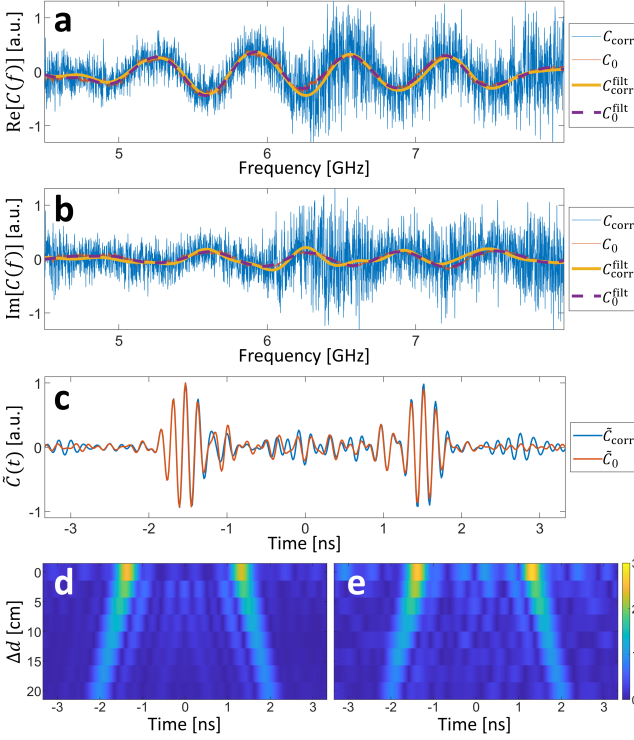


FIG. 2. (a,b) Real (a) and imaginary (b) part of reconstructed signal $C_{\text{corr}}(f)$ (blue) and benchmark signal $C_0(f)$ (red) in the frequency domain, as well as temporally filtered versions thereof. (c) Temporal signals corresponding to (a). (d,e) Envelope of the benchmark (d) and reconstructed (e) impulse response as a function of the variation of the distance Δd between the two antennas under test.

Inspired by the success of 1-bit time-reversal techniques⁴⁴, in a second step we therefore discard amplitude information by working with $S'_{13}(f) = \exp(j \arg(S'_{13}(f)))$ and $S''_{23}(f) = \exp(j \arg(S''_{23}(f)))$. These quantities are then used in Eq. (2): $C_{\text{corr}}(f) = \langle S'_{13}(f) S''_{23}{}^*(f) \rangle$.

In Fig. 2(a,b) we present the normalized real and imaginary parts of $C_{\text{corr}}(f)$ and the corresponding $C_0(f)$. While important details like amplitude variations, phase and envelope of both signals appear to be in good agreement, $C_{\text{corr}}(f)$ appears to be much noisier than $C_0(f)$. To understand this observation, we transform both signals to the time domain via an inverse Fourier transform. In Fig. 2(c) we present the resulting time-domain signal, labelled $\tilde{C}(t)$, which reveals excellent agreement between the ballistic components of $\tilde{C}_{\text{corr}}(t)$ and $\tilde{C}_0(t)$. The causal and anticausal parts of $\tilde{C}(t)$ are almost symmetrical, as expected since both antennas under test are nominally identical³⁰. The excellent agreement between $\tilde{C}_{\text{corr}}(t)$ and $\tilde{C}_0(t)$ is only observed within the pulse corresponding to the direct response between the antennas which explains the noise on the $C_{\text{corr}}(f)$ signal seen in Fig. 2(a,b). By applying a temporal filter to $\tilde{C}_{\text{corr}}(t)$, such that only the signal at the short times shown in Fig. 2(c) remains, and then returning to the spectral domain, we obtain indeed a smooth signal $C_{\text{corr}}^{\text{filt}}$ in good agreement with $C_0(f)$ – see the dashed lines in Fig. 2(a,b).

In order to study the impact of the separation between the

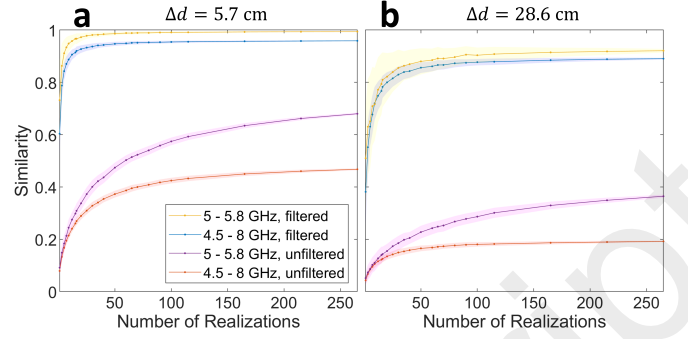


FIG. 3. Convergence of reconstructed signal toward the expected signal as a function of the number of utilized random metasurface configurations. For two different separations of the antennas under test, the convergence is shown for two different signal bandwidths and with or without temporal filtering. The shaded area indicates the standard deviation over 250 runs.

two antennas under test on the quality of the reconstructed signal, we repeated the above experiment for different separations. The corresponding envelopes of $\tilde{C}_0(t)$ and $\tilde{C}_{\text{corr}}(t)$ are shown in Fig. 2(d) and Fig. 2(e), respectively. The symmetry between causal and anticausal response is again clearly visible. The reconstruction quality slightly deteriorates as the separation Δd between the two antennas under test increases. For a large separation between the antennas, the signal to noise ratio (SNR) of the DFCC technique is inherently limited by the number of random configurations over which we average the correlation. The strength of the impulse response we are aiming to reconstruct decreases with the separation between the antennas so that the peak value of $\tilde{C}_{\text{corr}}(t)$ progressively converges towards the noise level of the correlation function.

We now investigate how the reconstruction quality depends on the size of the ensemble of random metasurface configurations. For two representative scenarios in which the antennas under test are quite close and quite far from each other, we plot the convergence of the similarity of $C_{\text{corr}}(f)$ and $C_0(f)$ (evaluated with Pearson's correlation coefficient) in Fig. 3. First, as expected, the filtered signals achieve a higher similarity value because the noise due to the poor reconstruction at long times is removed. Second, we see that the achievable similarity is slightly higher if the frequencies are restricted to the metasurface's nominal operation band; outside the 5–5.8 GHz band, the stirring efficiency is drastically lower such that ultimately the SNR of the measurement of the stirred field is significantly lower. Third, as already observed in Fig. 2(e), the reconstruction quality is higher the closer the antennas under test are to each other. Again, this can be related to the SNR: if the antennas are further apart, the direct signal is weaker and hence the reconstructed response suffers from a lower SNR. Overall, these observations highlight the critical role of SNR in DFCC; in our experiment, the inefficient stirring (especially outside the metasurface's operation band) and the separation between the two antennas under test strongly affect the SNR.

We have established the passive reconstruction of the impulse response in a metasurface-programmable complex scattering enclosure. This technique paves the way to characteriz-

ing the efficiency or directivity of antennas that are solely used in their receiving modes. We now extend our approach to an imaging scenario for which we aim to determine the location of an electromagnetic object (here a metallic trihedron) with a synthetic array of receiving antennas (see SM). The practical relevance thereof is found in sensing for context-awareness. The latter is often sought in complex scattering enclosures such as indoor environments, e.g., for ambient-assisted living^{45,46}, and at microwave frequencies often illuminators of opportunity can be exploited^{47–49}. For 200 random metasurface configurations, we measure the signal $S_{12}(f)$ generated by the source and captured by a horn antenna for 20 positions of the latter along the y -axis with steps of $\delta y_a = 1.842$ cm, forming a virtual aperture of $\Delta y_a = 0.35$ cm. For each position y_a , we compute the auto-correlation of $S'_{12}(f, y_a)$ and average it over the 200 realizations: $C_{\text{corr}}^w(f, y_a) = \langle |S_{12}(f, y_a) - \langle S_{12}(f, y_a) \rangle|^2 \rangle$. In order to remove the contributions of the RC that are not associated with the target, we use a differential approach. To that end, we repeat the same procedure to determine $C_{\text{corr}}^{wo}(f, y_a)$ in absence of the target. Finally, we consider the difference of the two: $C(f, y_a) = C_{\text{corr}}^w(f, y_a) - C_{\text{corr}}^{wo}(f, y_a)$.

We present in Fig. 4(a) the correlation $\tilde{C}(t, y_a)$ obtained via an inverse Fourier transform of $C(f, y_a)$ for an antenna facing the target. In addition to the pulse centered on $t = 0$ which is related to the auto-correlation of the field, two pulses emerge symmetrically at positive and negative times, corresponding to a distance of 0.9 m that can be associated with the target's contribution. We finally obtain an image $\mathcal{J}(\vec{r})$, where $\vec{r} = [x; y]$, with standard beamforming of $\tilde{C}(t, y_a)$ in the time domain: $\mathcal{J}(\vec{r}) = \int_{\Delta y_a} \tilde{C}(t, y_a) \delta(t - 2r_a/c_0) dy_a$, where $r_a = \sqrt{x^2 + (y - y_a)^2}$. The images shown in Fig. 4(b) for three different trihedron positions illustrate the capabilities of our approach to detect and localize a target. Note that a shadow contribution of the wall resulting from our differential imaging technique appears at a distance of 1.2 m in Fig. 4(a,b) which is consistent with the distance between the antenna array and the wall. This contribution in the target's direction corresponds to the part of the wall which is hidden by the target in the first step and hence appears after subtracting the contribution in absence of the target.

The above-described imaging protocol relies on access to phase and amplitude of the measured field in order to evaluate $\langle S_{12}(f, y_a) \rangle$ and hence find $S'_{12}(f, y_a)$. With an efficient stirring process, $\langle S_{12}(f, y_a) \rangle \rightarrow 0$ and $S_{12}(f, y_a) \rightarrow S'_{12}(f, y_a)$. Phase information is therefore only necessary in cases of inefficient stirring as in our setup. In contrast to phaseless imaging techniques that require elaborate algorithms to retrieve the phase information^{50,51}, the latter is encapsulated in the broadband auto-correlation function assuming an isotropic illumination and the stirring process. With the advent of "reconfigurable intelligent surfaces" covering large parts of our indoor environments to enhance wireless communication¹⁷, we faithfully expect that efficient all-electronic stirring will soon be within reach.

To demonstrate the feasibility of phaseless imaging with our DFCC technique, we now replace the metasurface-enabled electronic stirring with a mechanical stirring mechanism of much higher efficiency: two large mutually orthog-

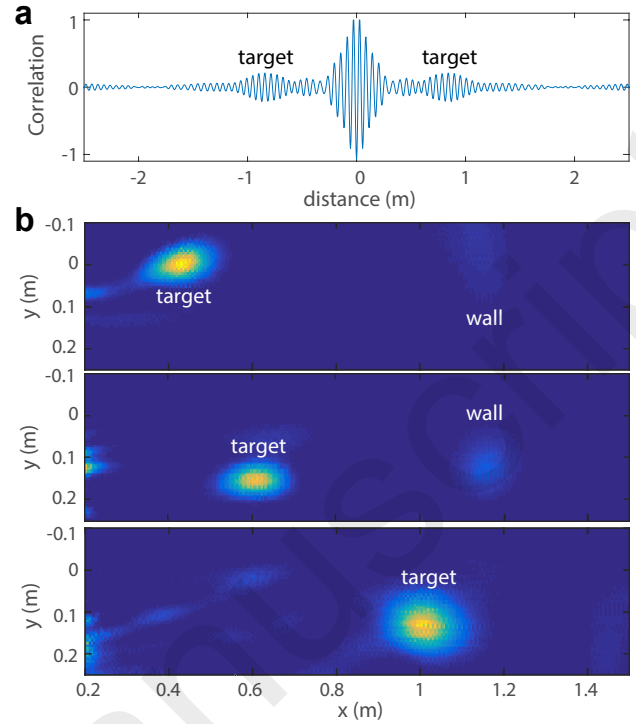


FIG. 4. (a) Correlation of $\tilde{C}(t, y_a)$ in the time domain for an antenna facing the metallic target as a function of the distance $d = c_0 t$. The contribution of the target appears at a distance of $2r_a = 0.85$ m. (b) Images of the target at three different positions obtained from beamforming of the back-propagation of $\tilde{C}(t, y_a)$ in the time domain.

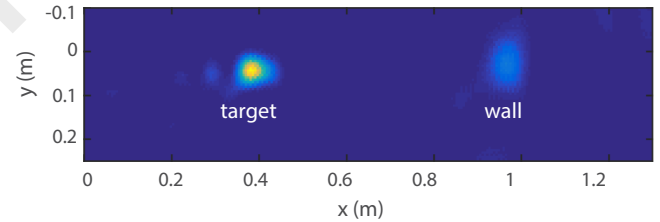


FIG. 5. Phaseless DFCC-based imaging of a metallic target located at a distance of 0.18 m from the virtual antenna array based on efficient mechanical mode-stirring. The auto-correlation is averaged over 50 stirrer configurations.

onal mode-stirrers that rotate within the RC – see Fig. 1(a). The stirred components now dominate over the unstirred components: $\langle |S_{12}(f, y_a)|^2 \rangle / \langle |S_{12}(f, y_a)|^2 \rangle = 0.05$. In Fig. 5, we report the imaging of the same target from beamforming of intensity-only measurements based on $\langle |S'_{12}(f, y_a)|^2 \rangle - \langle |S_{12}^{wo}(f, y_a)|^2 \rangle$.

In conclusion, we have shown that using programmable metasurfaces for electronic mode stirring in a reverberation chamber opens up new ways for the characterization of electromagnetic antennas and objects. By cross-correlating the field measured by two antennas in their receiving modes, we have reconstructed the impulse response between these two antennas. This approach is of great interest not only in the

context of electromagnetic compatibility but also for phase-less imaging techniques based on intensity measurements in indoor environments. Note that rather than changing the field's boundary conditions as in our present work, one can also apply source stirring⁵² to access an ensemble of field configurations, for instance, using a dynamic metasurface antenna as in Ref. 24.

This publication was supported by the French Agence Nationale de la Recherche under reference ANR-17-ASTR-0017, the European Union through the European Regional Development Fund (ERDF), by the French region of Brittany and Rennes Métropole through the CPER Project SOPHIE/STIC & Ondes. M.D. acknowledges the Institut Universitaire de France (IUF). The metasurface prototypes were purchased from Greenerwave.

Data is available on request from the authors.

- ¹D. F. Sievenpiper, J. H. Schaffner, H. J. Song, R. Y. Loo, and G. Tangonan, "Two-dimensional beam steering using an electrically tunable impedance surface," *IEEE Trans. Antennas Propag.* **51**, 2713–2722 (2003).
- ²C. L. Holloway, M. A. Mohamed, E. F. Kuester, and A. Dienstfrey, "Reflection and transmission properties of a metafilm: With an application to a controllable surface composed of resonant particles," *IEEE Trans. Electromagn. Compat.* **47**, 853–865 (2005).
- ³T. J. Cui, M. Q. Qi, X. Wan, J. Zhao, and Q. Cheng, "Coding metamaterials, digital metamaterials and programmable metamaterials," *Light Sci. Appl.* **3**, e218–e218 (2014).
- ⁴N. Kaina, M. Dupré, M. Fink, and G. Lerosey, "Hybridized resonances to design tunable binary phase metasurface unit cells," *Opt. Express* **22**, 18881–18888 (2014).
- ⁵H. Yang, X. Cao, F. Yang, J. Gao, S. Xu, M. Li, X. Chen, Y. Zhao, Y. Zheng, and S. Li, "A programmable metasurface with dynamic polarization, scattering and focusing control," *Sci. Rep.* **6**, 35692 (2016).
- ⁶F. Liu, O. Tsilipakos, A. Ptilakis, A. C. Tasolamprou, M. S. Mirmoosa, N. V. Kantartzis, D.-H. Kwon, M. Kafesaki, C. M. Soukoulis, and S. A. Tretyakov, "Intelligent metasurfaces with continuously tunable local surface impedance for multiple reconfigurable functions," *Phys. Rev. Applied* **11**, 044024 (2019).
- ⁷N. Engheta and R. W. Ziolkowski, *Metamaterials: Physics and Engineering Explorations* (John Wiley & Sons, 2006).
- ⁸T. J. Cui, D. R. Smith, and R. Liu, *Metamaterials* (Springer, 2010).
- ⁹F. Capolino, *Theory and Phenomena of Metamaterials* (CRC Press, 2017).
- ¹⁰L. Li, T. J. Cui, W. Ji, S. Liu, J. Ding, X. Wan, Y. B. Li, M. Jiang, C.-W. Qiu, and S. Zhang, "Electromagnetic reprogrammable coding-metasurface holograms," *Nat. Commun.* **8**, 1–7 (2017).
- ¹¹L. Li and T. J. Cui, "Information metamaterials—from effective media to real-time information processing systems," *Nanophotonics* **8**, 703–724 (2019).
- ¹²M. Dupré, P. del Hougne, M. Fink, F. Lemoult, and G. Lerosey, "Wave-Field Shaping in Cavities: Waves Trapped in a Box with Controllable Boundaries," *Phys. Rev. Lett.* **115**, 017701 (2015).
- ¹³P. del Hougne, F. Lemoult, M. Fink, and G. Lerosey, "Spatiotemporal Wave Front Shaping in a Microwave Cavity," *Phys. Rev. Lett.* **117**, 134302 (2016).
- ¹⁴M. F. Imani, D. R. Smith, and P. del Hougne, "Perfect absorption in a disordered medium with programmable meta-atom inclusions," *Adv. Funct. Mater.* **TBA**, 2005310 (2020).
- ¹⁵L. Subrt and P. Pechac, "Intelligent walls as autonomous parts of smart indoor environments," *IET Commun.* **6**, 1004–1010 (2012).
- ¹⁶P. del Hougne, M. Fink, and G. Lerosey, "Optimally diverse communication channels in disordered environments with tuned randomness," *Nat. Electron.* **2**, 36–41 (2019).
- ¹⁷C. Huang, A. Zappone, G. C. Alexandropoulos, M. Debbah, and C. Yuen, "Reconfigurable intelligent surfaces for energy efficiency in wireless communication," *IEEE Trans. Wirel. Commun.* **18**, 4157–4170 (2019).
- ¹⁸P. del Hougne, M. Fink, and G. Lerosey, "Shaping microwave fields using nonlinear unsolicited feedback: Application to enhance energy harvesting," *Phys. Rev. Applied* **8**, 061001 (2017).
- ¹⁹P. del Hougne and G. Lerosey, "Leveraging Chaos for Wave-Based Analog Computation: Demonstration with Indoor Wireless Communication Signals," *Phys. Rev. X* **8**, 041037 (2018).
- ²⁰M. Klingler, "Dispositif et procédé de brassage électromagnétique dans une chambre réverbérante à brassage de modes," Patent FR 2, 337 (2005).
- ²¹R. Serra, A. C. Marvin, F. Moglie, V. M. Primiani, A. Cozza, L. R. Arnaut, Y. Huang, M. O. Hatfield, M. Klingler, and F. Leferink, "Reverberation chambers a la carte: An overview of the different mode-stirring techniques," *IEEE Electromagn. Compat. Mag.* **6**, 63–78 (2017).
- ²²J.-B. Gros, P. del Hougne, and G. Lerosey, "Tuning a regular cavity to wave chaos with metasurface-reconfigurable walls," *Phys. Rev. A* **101**, 061801(R) (2020).
- ²³T. Sleasman, M. F. Imani, J. N. Gollub, and D. R. Smith, "Microwave Imaging Using a Disordered Cavity with a Dynamically Tunable Impedance Surface," *Phys. Rev. Applied* **6**, 054019 (2016).
- ²⁴P. del Hougne, M. F. Imani, T. Sleasman, J. N. Gollub, M. Fink, G. Lerosey, and D. R. Smith, "Dynamic metasurface aperture as smart around-the-corner motion detector," *Sci. Rep.* **8**, 1–10 (2018).
- ²⁵P. del Hougne, M. F. Imani, M. Fink, D. R. Smith, and G. Lerosey, "Precise Localization of Multiple Noncooperative Objects in a Disordered Cavity by Wave Front Shaping," *Phys. Rev. Lett.* **121**, 063901 (2018).
- ²⁶R. L. Weaver and O. I. Lobkis, "Ultrasonics without a source: Thermal fluctuation correlations at MHz frequencies," *Phys. Rev. Lett.* **87**, 134301 (2001).
- ²⁷O. I. Lobkis and R. L. Weaver, "On the emergence of the Green's function in the correlations of a diffuse field," *J. Acoust. Soc. Am.* **110**, 3011–3017 (2001).
- ²⁸M. Campillo and A. Paul, "Long-range correlations in the diffuse seismic coda," *Science* **299**, 547–549 (2003).
- ²⁹M. Davy, M. Fink, and J. de Rosny, "Green's function retrieval and passive imaging from correlations of wideband thermal radiations," *Phys. Rev. Lett.* **110**, 203901 (2013).
- ³⁰M. Davy, J. de Rosny, and P. Besnier, "Green's function retrieval with absorbing probes in reverberating cavities," *Phys. Rev. Lett.* **116**, 213902 (2016).
- ³¹U. Kuhl, "Wave functions, nodal domains, flow, and vortices in open microwave systems," *Eur. Phys. J. Special Topics* **145**, 103 (2007).
- ³²J.-B. Gros, U. Kuhl, O. Legrand, F. Mortessagne, O. Picon, and E. Richalot, "Statistics of the electromagnetic response of a chaotic reverberation chamber," *Adv. Electromagn.* **4**, 38 (2015).
- ³³J.-B. Gros, U. Kuhl, O. Legrand, and F. Mortessagne, "Lossy chaotic electromagnetic reverberation chambers: Universal statistical behavior of the vectorial field," *Phys. Rev. E* **93**, 032108 (2016).
- ³⁴B. Van Tiggelen, "Green function retrieval and time reversal in a disordered world," *Phys. Rev. Lett.* **91**, 243904 (2003).
- ³⁵R. Snieder, "Extracting the green's function from the correlation of coda waves: A derivation based on stationary phase," *Phys. Rev. E* **69**, 046610 (2004).
- ³⁶E. Larose, L. Margerin, A. Derode, B. van Tiggelen, M. Campillo, N. Shapiro, A. Paul, L. Stehly, and M. Tanter, "Correlation of random wavefields: An interdisciplinary review," *Geophys.* **71**, S111–S121 (2006).
- ³⁷R. Snieder, Y. Fan, E. Slob, and K. Wapenaar, "Equipartitioning is not sufficient for green's function extraction," *Earthq. Sci.* **23**, 403–415 (2010), 1674-4519.
- ³⁸J. de Rosny and M. Davy, "Green's function retrieval and fluctuations of cross density of states in multiple-scattering media," *EPL* **106**, 54004 (2014).
- ³⁹L. Chehami, J. de Rosny, C. Prada, E. Moulin, and J. Assaad, "Experimental study of passive defect localization in plates using ambient noise," *IEEE Trans. Ultrason. Ferroelectr. Freq. Control* **62**, 1544–1553 (2015).
- ⁴⁰A. Hejazi Nooghabi, L. Boschi, P. Roux, and J. de Rosny, "Coda reconstruction from cross-correlation of a diffuse field on thin elastic plates," *Phys. Rev. E* **96**, 032137 (2017).
- ⁴¹J. Garnier and G. Papanicolaou, *Passive Imaging with Ambient Noise* (Cambridge University Press, 2016).
- ⁴²S. M. Rytov, Y. A. Kravtsov, and V. I. Tatarskii, *Principles of Statistical Radiophysics 3: Elements of Random Fields* (Springer, New York, 1989).
- ⁴³P. del Hougne, D. V. Savin, O. Legrand, and U. Kuhl, "Implementing non-

- universal features with a random matrix theory approach: Application to space-to-configuration multiplexing,” *Phys. Rev. E* **102**, 010201(R) (2020).
- ⁴⁴A. Derode, A. Tourin, and M. Fink, “Ultrasonic pulse compression with one-bit time reversal through multiple scattering,” *J. Appl. Phys.* **85**, 6343–6352 (1999).
- ⁴⁵A. Hristova, A. M. Bernardos, and J. R. Casar, “Context-aware services for ambient assisted living: A case-study,” in *2008 First International Symposium on Applied Sciences on Biomedical and Communication Technologies* (IEEE, 2008) pp. 1–5.
- ⁴⁶P. Rashidi and A. Mihailidis, “A survey on ambient-assisted living tools for older adults,” *IEEE J. Biomed. Health Inform.* **17**, 579–590 (2012).
- ⁴⁷J. Palmer, S. Palumbo, A. Summers, D. Merrett, S. Searle, and S. Howard, “An overview of an illuminator of opportunity passive radar research project and its signal processing research directions,” *Digit. Signal Process.* **21**, 593–599 (2011).
- ⁴⁸D. Gromek, K. Kulpa, and P. Samczyński, “Experimental results of passive sar imaging using dvb-t illuminators of opportunity,” *IEEE Geosci. Remote. Sens. Lett.* **13**, 1124–1128 (2016).
- ⁴⁹P. M. Holl and F. Reinhard, “Holography of wi-fi radiation,” *Phys. Rev. Lett.* **118**, 183901 (2017).
- ⁵⁰A. Chai, M. Moscoso, and G. Papanicolaou, “Array imaging using intensity-only measurements,” *Inverse Problems* **27**, 015005 (2010).
- ⁵¹E. J. Candes, Y. C. Eldar, T. Strohmer, and V. Voroninski, “Phase retrieval via matrix completion,” *SIAM Review* **57**, 225–251 (2015).
- ⁵²G. Cerri, V. M. Primiani, S. Pennesi, and P. Russo, “Source stirring mode for reverberation chambers,” *IEEE Trans. Electromagn. Compat.* **47**, 815–823 (2005).